Received: 9 September 2021 | Revised: 13 October 2021 | Accepted: 19 October 2021

DOI: 10.1002/glia.24110

GLIA

WILEY

RESEARCH ARTICLE

Inhibition of monoamine oxidase B prevents reactive astrogliosis and scar formation in stab wound injury model

Heejung Chun[1] | Jiwoon Lim[1,2] | Ki Duk Park[3,4] | C. Justin Lee[1,2]

[1]Center for Cognition and Sociality, Institute for Basic Science (IBS), Daejeon, Republic of Korea

[2]IBS School, University of Science and Technology (UST), Daejeon, Republic of Korea

[3]Convergence Research Center for Diagnosis, Treatment and Care System of Dementia, Korea Institute of Science and Technology, Seoul, Republic of Korea

[4]Division of Bio-Med Science & Technology, KIST School, Korea University of Science and Technology (UST), Seoul, Republic of Korea

Correspondence
C. Justin Lee, Center for Cognition and Sociality, Institute for Basic Science (IBS), Daejeon 34126, Republic of Korea.
Email: cjl@ibs.re.kr

Funding information
Institute for Basic Science, Grant/Award Number: IBS-R001-D2

Abstract

Reactive astrocytes manifest molecular, structural, and functional alterations under various pathological conditions. We have previously demonstrated that the reactive astrocytes of the stab wound injury model (STAB) display aberrant cellular gamma-aminobutyric acid (GABA) content and tonic GABA release, whereas the active astrocytes under enriched environment (EE) express high levels of proBDNF. However, the role of monoamine oxidase B (MAO-B) in reactive astrogliosis and hypertrophy still remains unknown. Here, we investigate the role of MAO-B, a GABA-producing enzyme, in reactive astrogliosis in STAB. We observed that the genetic removal of MAO-B significantly reduced the hypertrophy, scar formation, and GABA production of reactive astrocytes, whereas the MAO-B overexpression under glial fibrillary acidic protein (GFAP) promoter enhanced the levels of GFAP and GABA. Furthermore, we found that one of the by-products of the MAO-B action, H_2O_2, but not GABA, was sufficient and necessary for the hypertrophy of reactive astrocytes. Notably, we identified two potent pharmacological tools to attenuate scar-forming astrogliosis—the recently developed reversible MAO-B inhibitor, KDS2010, and an H_2O_2 scavenger, crisdesalazine (AAD-2004). Our results implicate that inhibiting MAO-B activity has dual beneficial effects in preventing astrogliosis and scar-formation under brain injury, and that the MAO-B/H_2O_2 pathway can be a useful therapeutic target with a high clinical potential.

KEYWORDS
brain injury, glial scar, H_2O_2, MAO-B, reactive astrocytes

1 | INTRODUCTION

Astrocytes, as the most abundant and ubiquitous cell type in the brain, play multiple and essential roles in the brain function. They dynamically change their properties when responding to various physiological and pathological stimuli. For decades, researchers have recognized that astrocytes show morphologically hypertrophied forms in various diseased conditions, which have been named 'reactive astrocytes' or 'astrogliosis'. In addition to morphological alterations, astrocytes exhibit various aspects of changes in the molecular or metabolic profiles, implying that there is heterogeneity of reactive astrocytes (Escartin et al., 2019; Escartin et al., 2021). Based on the criteria set for each study, several research groups have tried to categorize or define each subtype and proposed the functional consequences of these reactive astrocytes in each category. In particular, based on the molecular profiles of reactive astrocytes, one group of researchers have attempted to define the detrimental and beneficial reactive astrocytes as A1 or A2 in the LPS-induced or MCAO-stroke models, respectively (Liddelow et al., 2017). According to their claims and the follow-up studies, the distinct patterns of gene expression in LPS-induced A1 astrocytes can be correlated with molecular patterns shown in various neurodegenerative diseases such as Alzheimer's disease or Parkinson's disease (Li et al., 2019; Yun et al., 2018). However, the categorization of A1 and A2 types of reactive astrocytes has been

Heejung Chun and Jiwoon Lim contributed equally to this work.

challenged by a large consortium of researchers studying reactive astrocytes (Escartin et al., 2021), raising a concern that A1 and A2 categorization does not adequately represent the reactive astrocytes that are found in various human pathologies.

In contrast to the A1/A2 categorization, researchers suggested that reactive astrocytes show gradated continuum from resting to severe reactive astrocytes. In previous studies, we observed that reactive astrocytes share MAO-B-GABA pathway in various brain disease models such as penetrating brain injury model (Chun et al., 2018; Chun et al., 2020; Heo et al., 2020; Jo et al., 2014; Nam, Cho, et al., 2020). In addition, we recently reported that 'mild' and 'severe' reactive astrocytes can be distinguished by the degree of astrocyte's responses to toxic materials and share the common molecular pathway of MAO-B-GABA. In the same study, we reported that the reactive astrocytes acquire more detrimental function as the common MAO-B-GABA pathway is more activated and the reactivity of astrocytes become more severe (Chun et al., 2020). Furthermore, we demonstrated that the detrimental transformation of astrocytes is highly correlated with the action of MAO-B and the aberrant production of hydrogen peroxide (H_2O_2). However, it is still unknown whether scar-forming reactive astrocytes, which are known as the most severe form of reactive astrogliosis (Sofroniew, 2009), also share the molecular mechanism related to MAO-B/GABA/H_2O_2.

Glial scars are characterized by an inflammatory response to injury in the central nervous system (CNS). The scars primarily act as a barrier to the injured CNS from further infection, but are detrimental to tissue recovery by preventing the axonal regeneration of damaged neurons. The scar formation of astrocytes is a major component of this specialized tissue remodeling only observed in penetrating injured brain and includes astrocyte migration and astrocyte proliferation in the vicinity of the lesion (Matyash et al., 2002; McGraw et al., 2001). These plastic changes of astrocytes depend on the dynamics of the actin cytoskeleton and the integrity of the intermediate filament including vimentin and glial fibrillary acidic protein (GFAP) (Bourguignon et al., 2007; Menet et al., 2003). However, the molecular mechanisms underlying these structural alterations and the involvement of MAO-B-dependent H_2O_2 in hypertrophy and scar formation in reactive astrogliosis have not been investigated in detail.

MAO-B belongs to a family of flavin-containing monoamine oxidases and is located in the outer membrane of mitochondria. MAO-B catalyzes the oxidative deamination of biogenic monoamines such as dopamine or acetyl-putrescine, playing a key role in the regulation of monoaminergic neurotransmission (Tong et al., 2017; Yoon et al., 2014). MAO-B is majorly expressed in astrocytes (Ekblom et al., 1993) and produces GABA and H_2O_2 by oxidizing acetyl-putrescine (Maggiorani et al., 2017; Yoon et al., 2014). It is also known to be up-regulated in reactive astrocytes in various neurodegenerative diseases (Jo et al., 2014; Mallajosyula et al., 2008) and the resulting aberrant putrescine degradation pathway causes increased tonic GABA release and inhibits the synaptic activity of neighboring neurons. Furthermore, H_2O_2 overproduction triggers astrocytic transformation into severe reactive astrocyte by turning on iNOS expression, which is alleviated by ROS scavenger (Chun et al., 2020). Notably, the MAO-B inhibition rescues various aspects of brain malfunctions in animal models of Alzheimer's disease, Parkinson's disease and stroke and reverses the reactive astrogliosis or hypertrophy (Heo et al., 2020; Nam, Cho, et al., 2020; Park et al., 2019). However, the detailed molecular pathway underlying the involvement of MAO-B in morphological alteration remains elusive.

In this study, we investigated the molecular mechanisms underlying MAO-B-mediated morphological hypertrophy in reactive astrocytes. We adopted stab wound injury model (STAB), an animal model of penetrating traumatic brain injury, which can induce reactive astrocytes in a graded fashion, ranging from proliferating scar-forming reactive astrocytes to mild/moderate reactive astrocytes (Sofroniew, 2009). We employed unbiased imaging technology to visualize scar-forming severe reactive astrocytes as a 3-dimensional (3D) object by 3D reconstruction and to quantify the branching level of astrocyte processes using Imaris software. Our study used genetic animal models of MAO-B knock-out and MAO-B overexpression mouse models in addition to the latest pharmacological tools of the recently developed reversible MAO-B inhibitor, KDS2010, and a H_2O_2 scavenger, crisdesalazine (AAD-2004). We demonstrated that H_2O_2, a by-products of MAO-B activation induces hypertrophy and scar formation in reactive astrocytes.

2 | METHODS

2.1 | Animals and housing

All animal care and handling procedures were performed in accordance with the Institutional Animal Care and Use Committee of IBS (Daejeon, Korea). Each mouse line was originated from the Jackson Laboratory (USA, stock number 000664 for C57BL/6J mice, 014133 for MAO-B KO mice (B6;129S-Maobtm1Shih/J) and 017955 for hGFAP-MAO-B mice (C57BL/6-Tg(Gfap-rtTA,tetO-MAOB,-lacZ)1Jkan/J)). All animals were housed three to five per cage. Mice had free access to food and water and were maintained on a 12-h light–dark cycle. All experiments were done with sex- and age-matched controls.

2.2 | Primary cortical astrocytes

Primary cortical astrocytes were prepared from postnatal day (P) P0–P3 C57BL/6 mice. The cerebral cortex was dissected free of adherent meninges, minced and dissociated into single-cell suspension by trituration. Cells were grown in DMEM (Invitrogen) supplemented with 25 mM of glucose, 10% heat-inactivated horse serum, 10% heat-inactivated FCS, 2 mM of glutamine and 1000 U ml^{-1} penicillin–streptomycin. Cultures were maintained at 37°C in a humidified 5% CO_2 incubator. On the third day of culture, cells were vigorously washed with repeated pipetting and the medium was replaced to get rid of debris and other floating cell types.

2.3 | Stab wound brain injury

Animals were deeply anesthetized with isoflurane and mounted in a stereotaxic frame. The scalp was incised, and a hole was drilled into the skull above the hippocampal CA1 region (AP, −2 mm; ML, −1.5 mm from the bregma). Then, a 23-gauge needle was slowly inserted into the brain, penetrating the hippocampus (DV 3 mm from dura), left for 20 min, and then slowly retracted. The contralateral side served as the no-injury control. One week after surgery, the mice were sacrificed for immunostaining.

2.4 | Drug treatment

For drinking experiments, KDS2010 was dissolved in water at a dose of 10 mg/kg. Crisdesalazine (AAD-2004, supplied by GNT Pharma) was dissolved in DMSO at a concentration of 500 mM for the stock solution. For the working solution, the stock solution was diluted in PBS at a concentration of 1 mM and mice were intraperitoneally injected at 3.3 mg/kg.

2.5 | Immunohistochemistry

Animals were deeply anesthetized using 2% avertin and perfused with 0.1 M PBS, followed by 4% paraformaldehyde solution. Brains were post-fixed in 4% paraformaldehyde at 4°C for 24 h and dehydrated in 30% sucrose at 4°C for 24 h. Cryosection of the brain was performed in the coronal section (30 μm). Samples were blocked in 0.1 M PBS containing 0.3% Triton X-100 (Sigma) and 4% donkey serum (Genetex) for 2 h at room temperature. The primary antibodies used were as follows: chicken anti-GFAP (1:500, ab5541, Millipore) and guinea pig anti-GABA (1:200, ab175, Millipore). Samples with primary antibodies were incubated overnight at 4°C. The sections were then washed three times in 0.1 M PBS and incubated with appropriate secondary antibodies (1:200) from the Jackson Laboratory for 3 h. After three rinses in 0.1 M PBS and DAPI staining at 1:1000 (PIERCE), the samples were mounted on a Polysine microscopic slide glass (Thermo Scientific). Images were acquired using a Nikon A1R confocal microscope and Zeiss LSM 900 microscope.

2.6 | Western blot

Cultured cortical astrocytes were lysed with RIPA buffer (#MB-030-0050, Rockland) containing protease and phosphatase inhibitor cocktail (#1861281, Thermo Fisher). Protein lysates (20 mg) were separated by protein electrophoresis using protein gels (#456-1084, Bio-Rad) and blotted onto PVDF membranes (#IB24001, Thermo Fisher). The blots were incubated overnight at 4°C with chicken anti-GFAP (#AB5541, Millipore, 1:1000) or mouse anti-GAPDH (#ab8245, Abcam, 1:3000). Blots were then washed and incubated with horseradish peroxidase(HRP)-conjugated rabbit anti-chicken IgY (#AP162P, Millipore) or anti-mouse IgG (#NIF825m, Amersham), followed by washing and detection of immunoreactivity with enhanced chemiluminescence (#1705061, Bio-Rad). The band intensity was acquired using ImageQuant LAS 500 (#29005063, GE Healthcare Life Sciences) and quantified using ImageJ software (NIH).

2.7 | Image analysis and quantification

Microscopic images were analyzed using the ImageJ software (NIH). To measure GABA intensity in astrocytes, GFAP images were converted into a binary file, and GFAP+ astrocytes were selected as regions of interest (ROIs). Then, the mean intensity value of GABA in each ROI was measured. To analyze the total GABA content in one astrocyte, the average intensity of GABA in each GFAP+ astrocyte was multiplied by the area of the GFAP-positive region.

2.8 | Imaris surface analysis

Raw image files were used for further analysis using Imaris software (Version 9.0.1, Oxford Instruments). First, manual surface reconstruction was used to obtain the stratum radiatum region of the hippocampus, and GFAP signals were masked with the reconstructed surface of the stratum radiatum. Then, the astrocyte surface was reconstructed with a newly created GFAP channel. Because we used different confocal settings for different experimental conditions, different custom settings were applied. The parameters were: surface details: 0.621 μm (smooth); manual threshold value min: 500; diameter of largest sphere: 2.33; color: base, diffusion transparency: 65% for KDS2010 and crisdesalazine-treated batch; surface detail: 0.621 μm (smooth); manual threshold value min: 600; diameter of largest sphere: 2.33; color: base, diffusion transparency: 65% for MAO-B knock out batch. Surface details: 0.624 μm (smooth); manual threshold value min: 15; diameter of largest sphere: 2.34; color: base, diffusion transparency: 65% for MAO-B overexpression batch. After reconstruction, we used the filter function to remove non-specific background signals and incomplete cells; filter: volume min 350 μm^3. After reconstruction, GABA signals in the GFAP surface was obtained by 'mask all' function.

2.9 | Imaris filament analysis

Sholl analysis was performed using Imaris in the filament reconstruction mode. We used different parameters for different batches of images to ensure that the reconstructed filament represented the GFAP signal properly. The parameters were: detect new starting points: largest diameter 8.00 μm, seed points 0.5 μm; remove seed points around starting points: diameter of sphere regions: 16 μm for contralateral vs. ipsilateral batch, KDS2010 and crisdesalazine-treated

batch and MAO-B overexpression batch; 10.00 μm, seed point 1 μm; remove seed points around starting points; diameter of sphere regions; 20 μm for MAO-B knock out batch. After reconstruction, false signals were removed with a filter function: filter: filament area min 100 μm^2. All images of the same batch were taken using the same confocal settings. Image processing, three-dimensional reconstruction, and data analyses were performed in a blinded manner with respect to the experimental conditions.

2.10 | Statistical analysis

The statistical significance of data for comparison was assessed by Student's two-tailed unpaired *t*-test between two groups and one-way ANOVA test between three or more groups. Analyses were performed using Prism software (GraphPad Software, Inc.). Data distribution was assumed to be normal, but was not formally tested. Data are presented as the mean ± SEM. Statistical significance was set to $p < 0.05$.

3 | RESULTS

3.1 | Visualization and quantitative analysis of astrocyte morphology in STAB

To visualize the morphological architecture of scar-forming reactive astrocytes in STAB, we induced penetrating injury in the mouse brain. After 1 week, we performed immunostaining for GFAP, an astrocyte-specific structural protein, and imaged using confocal microscopy (Figure 1a). Because the astrocytes presenting in almost all brain regions are heterogeneous in terms of shape and gene expression (Zhang & Barres, 2010), we selected the GFAP signals only in the stratum radiatum of the hippocampal CA1 region to minimize the possibility of regional heterogeneity of astrocytes. The stratum radiatum region was manually selected to create a surface that was used to mask the GFAP signals. The masked raw GFAP signals were reconstructed using a surface rendering in the Imaris software (Figure 1b,c). The 3D-rendered astrocytes were pseudo-colored based on the volume of each astrocyte in the STAB model. Through 3D rendering and color coding, the dramatic increase in scar-forming reactive astrocytes and morphological hypertrophy of astrocytes in the ipsilateral region of the STAB model could be clearly visualized (Figure 1c–f). Additionally, the immunostained GABA signals in the GFAP-positive area were markedly enhanced in the ipsilateral side compared to the contralateral side of the STAB model, as previously reported (Chun et al., 2018), and the GABA signals were masked by GFAP-surface to visualize the astrocytic GABA signals (Figure 1d,f).

To show the fine details of the morphological complexity of reactive astrocytes, we employed a filament-tracing algorithm in the Imaris software, which was originally designed for quantifying neuronal dendrites. We performed a Sholl analysis and measured several parameters to quantify the complexity of astrocyte's branching (e.g., the sum of process volume/length, the number of branching points, the full branch depth, the mean of segment length and the ending radius) (Figure 1g,l). On the ipsilateral side of STAB, astrocytes demonstrated a significant increase in the number of intersections, the sum of process volume/length, the number of branching points, the full branch depth, and the ending radius (Figure 1g–o). Moreover, the astrocytes in STAB showed a marked reduction in the mean of segment length, which is a distance between filament branch points, indicating a greater occurrence of branching points in the processes (Figure 1n). These data show that the reactive astrocytes triggered by STAB exhibit highly complex arborization of fine and branched processes. These analysis parameters make it possible to clearly demonstrate the quantitative assessment of astrocyte morphology.

3.2 | The effects of genetic manipulation of monoamine oxidase B on scar-forming reactive astrocytes in STAB

Previously, we have reported that astrocytic GABA, as well as GFAP, was markedly increased in reactive astrocytes near the injured region of STAB (Chun et al., 2018). We have also shown that the aberrant GABA in reactive astrocytes in AD, PD and stroke models is mediated by MAO-B activation (Heo et al., 2020; Jo et al., 2014; Nam, Cho, et al., 2020). Notably, MAO-B activity is associated with the severity of reactive astrocytes. Based on these previous reports, we investigated whether the increased levels of GABA and GFAP and the morphological hypertrophy of scar-forming severe reactive astrocytes in STAB is mediated by MAO-B activation, similar to the other cases of brain diseases. We examined the effect of MAO-B genetic modulation on the morphological hypertrophy of astrocytes in STAB model using mice with gene knockout or overexpression mice of MAO-B (MAO-B KO and hGFAP-MAO-B mice, respectively). First, we conducted STAB surgery on MAO-B KO mice and performed immunostaining with GFAP and GABA antibodies 1 week after brain injury (Figure 2a). With confocal imaging and 3D rendering, we observed that the intensity of GFAP and GABA signals near injured sites was significantly reduced in the MAO-B KO mice compared to wild-type (WT) mice (Figure 2b–d). Furthermore, filament tracing and Sholl analysis showed that the astrocytes in the KO mice displayed a significant reduction in astrocyte complexity compared to that in WT mice (Figure 2e–l). The number of intersections, sum of process volume/length, number of branching points, full branch depth and ending radius were significantly decreased in the KO condition compared to the WT condition (Figure 2g,h), whereas the mean segment length was not significantly different (Figure 2j–l). These results indicate that MAO-B is necessary for the induction of scar-forming severe reactive astrocytes in STAB.

Second, to investigate whether the increase in MAO-B activity can exacerbate the reactivity of astrocytes in STAB, we overexpressed MAO-B specifically in astrocytes under the control of

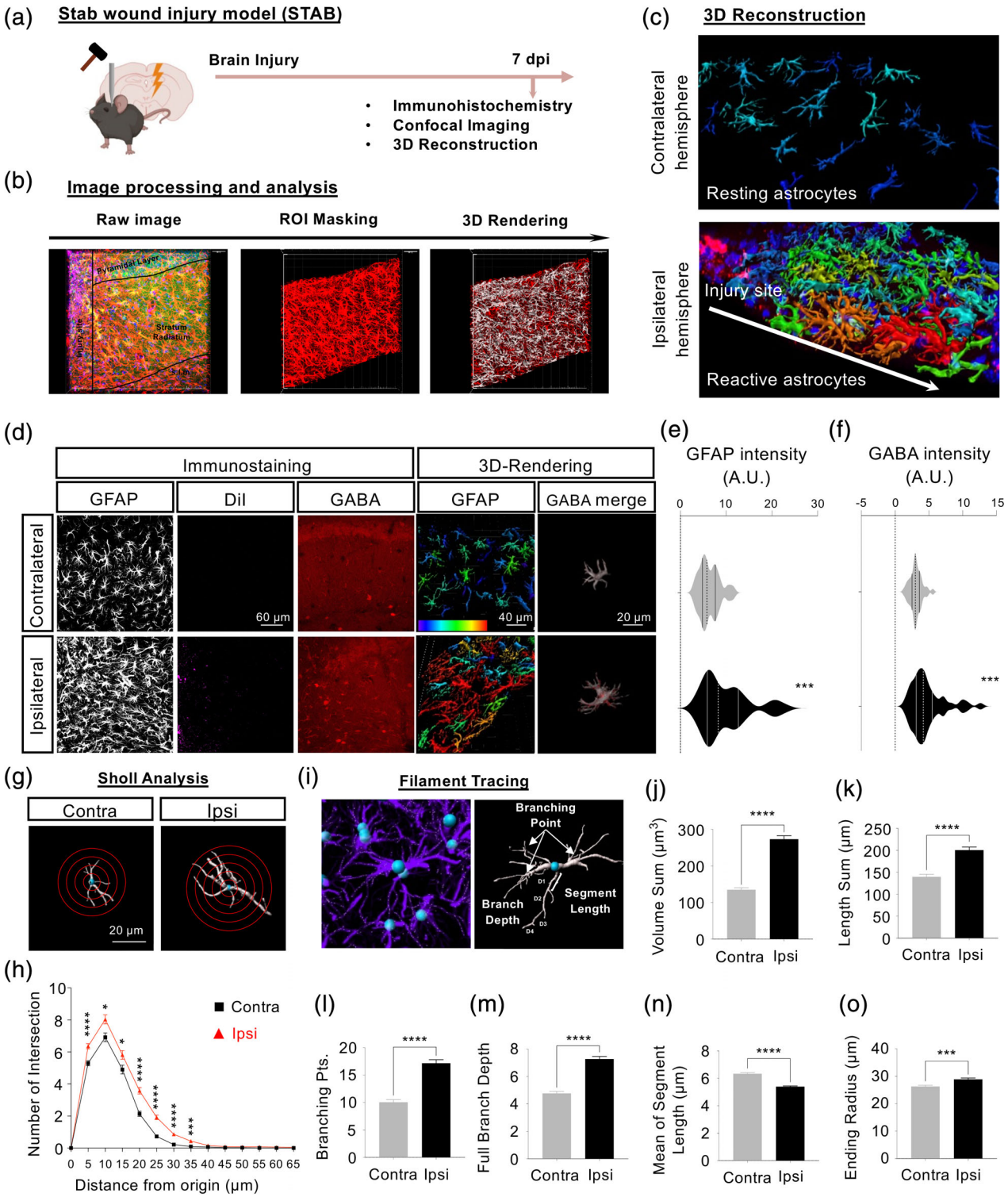

FIGURE 1 Experimental procedure and image analysis for stab wound injury (STAB) model. (a) Experimental timeline for generating STAB model. (b) 3D rendering procedure of astrocytes in CA1 stratum radiatum using immunostained images. (c) Representative image of 3D-rendered scar-forming reactive astrocytes in STAB model. (d) Representative confocal images for glial fibrillary acidic protein (GFAP), gamma-aminobutyric acid (GABA) and DiI (left) and the processed 3D-rendered images for GFAP pseudo-colored by volume (value range: 0–8000) and GABA (right) in STAB model. (e,f) Violin plot showing the average intensity for GFAP (e) and GABA (f) in contralateral and ipsilateral side of STAB brain. (g) Representative images of sholl analysis in astrocytes of STAB model. (h) Measurement of the number of intersection according to the distance from the nucleus through sholl analysis. (i) Filament tracing method in Imaris software to determine 'the number of branching points', 'the full process depth' and 'the mean segment length' of astrocyte processes. (j–o) Measurement of the volume sum (j), the length sum (k), the branching points (l), the full branch depth (m), the mean of segment length (n) and the ending radius (o). Data are presented as the mean ± SEM (*p < .05, ***p < .001, ****p < .0001)

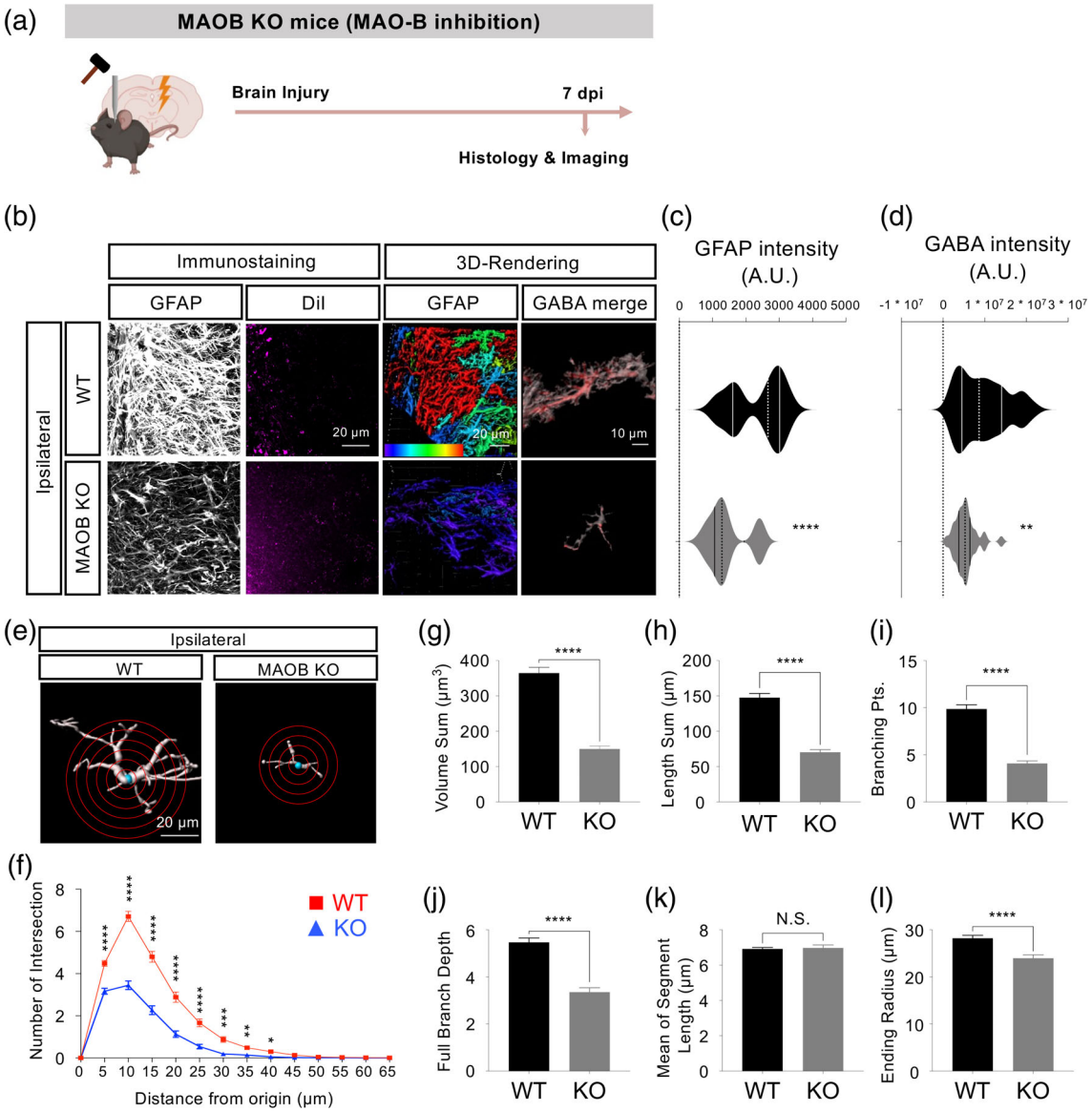

FIGURE 2 The morphological hypertrophy in scar-forming severe reactive astrocytes of STAB is attenuated in monoamine oxidase B (MAO-B) knockout (KO) mice. (a) Experimental timeline for STAB in MAO-B KO mice. (b) Representative confocal images for glial fibrillary acidic protein (GFAP) and DiI (left) and the 3D-rendered images for GFAP pseudo-colored by volume (value range: 0–8000) and gamma-aminobutyric acid (GABA) (right) in STAB model of MAO-B KO mice. (c,d) Violin plot showing the average intensity of GFAP (c) and GABA (d) immunoreactivity in CA1 stratum radiatum of MAOB-KO STAB model. (e) Representative images of sholl analysis in astrocytes of MAOB-KO STAB model. (f) Measurement of the number of intersection according to the distance from the nucleus through sholl analysis. (g–l) Measurement of the volume sum (g), the length sum (h), the branching points (i), the full branch depth (j), the mean of segment length (k) and the ending radius (l). Data are presented as the mean ± SEM (*p < .05, **p < .01, ***p < .001, ****p < .0001)

the GFAP promoter using hGFAP-MAO-B mice. To fully express MAO-B in each astrocyte, hGFAP-MAO-B mice were exposed to doxycycline chow for 3 weeks. After feeding doxycycline chow, we conducted STAB surgery on the hGFAP-MAOB mice and, compared the degree of astrocytic reactivity by measuring the intensity of GFAP and GABA signals near injury sites at 7 days after surgery (Figure 3a). Both GFAP and GABA signals were significantly increased in hGFAP-MAOB mice compared to WT mice and the overall volume of GFAP signals was increased (Figure 3b–d). However, the branching level of processes in each astrocyte was not different; rather, the process volume was significantly decreased in *Tg* mice compared to WT mice (Figure 3e–l). These results suggest that the additive expression of MAO-B in STAB increase the GFAP and GABA protein expression, while astrocytes become denser at their soma rather than having more complex branches in their morphology. Probably, these astrocytes appear to be going into an atrophic or senescence state beyond severe reactive astrocytes (Verkhratsky et al., 2019).

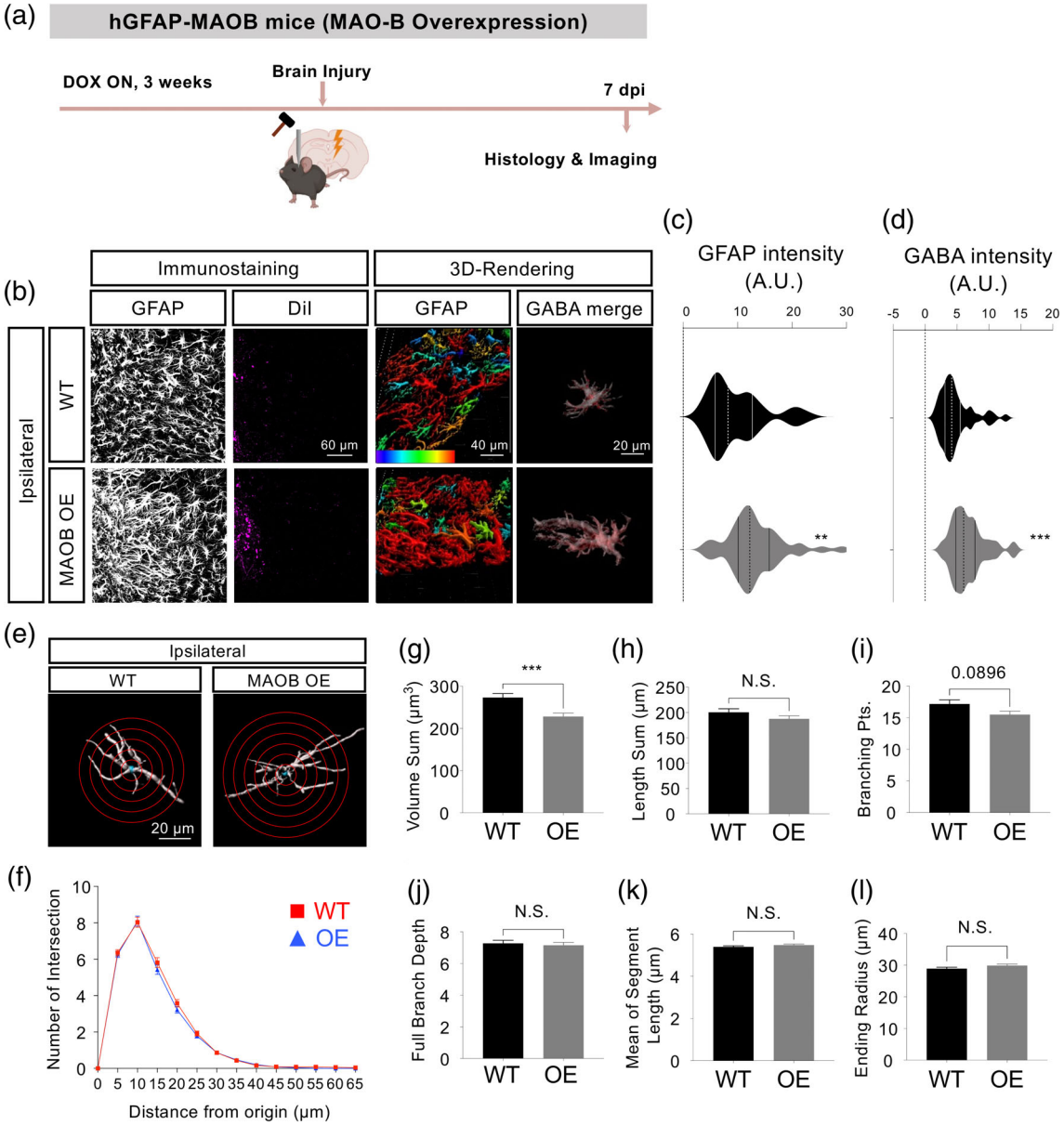

FIGURE 3 The overexpression of monoamine oxidase B (MAO-B) in astrocytes increases the molecular markers of reactive astrocytes in STAB. (a) Experimental timeline for STAB in hGFAP-MAOB mice. (b) Representative confocal images for GFAP and DiI (left) and the 3D-rendered images for glial fibrillary acidic protein (GFAP) pseudo-colored by volume (value range: 0–8000) and gamma-aminobutyric acid (GABA) (right) in STAB model of hGFAP-MAOB mice. (c,d) Violin plot showing the average intensity of GFAP (c) and GABA (d) immunoreacitivity in CA1 stratum radiatum of hGFAP-MAOB STAB model. (e) Representative images of sholl analysis in astrocytes of hGFAP-MAOB STAB model. (f) Measurement of the number of intersection according to the distance from the nucleus through sholl analysis. (g–l) Measurement of the volume sum (g), the length sum (h), the branching points (i), the full branch depth (j), the mean of segment length (k) and the ending radius (l). Data are presented as the mean ± SEM (**p < .01, ***p < .001)

3.3 | Pharmacological attenuation of scar-forming severe reactive astrocytes in STAB

It has long been recognized that glial scars act as a physical barrier to block axon regeneration of damaged neurons, which is believed to be associated with functional recovery (Sofroniew, 2009). Because our previous genetic study suggests that MAO-B is an effective target for manipulating glial scar formation, we adopted a recently developed potent MAO-B inhibitor, KDS2010, which has been reported to show dramatic functional recovery in experimental models of brain diseases such as Parkinson's disease, stroke and Alzheimer's disease (Nam, Cho, et al., 2020; Nam, Park, et al., 2021; Park et al., 2019). We administered the KDS2010 (10 mg/kg/day) orally for 7 days immediately after STAB surgery and sacrificed the mice for immunohistochemistry (Figure 4a).

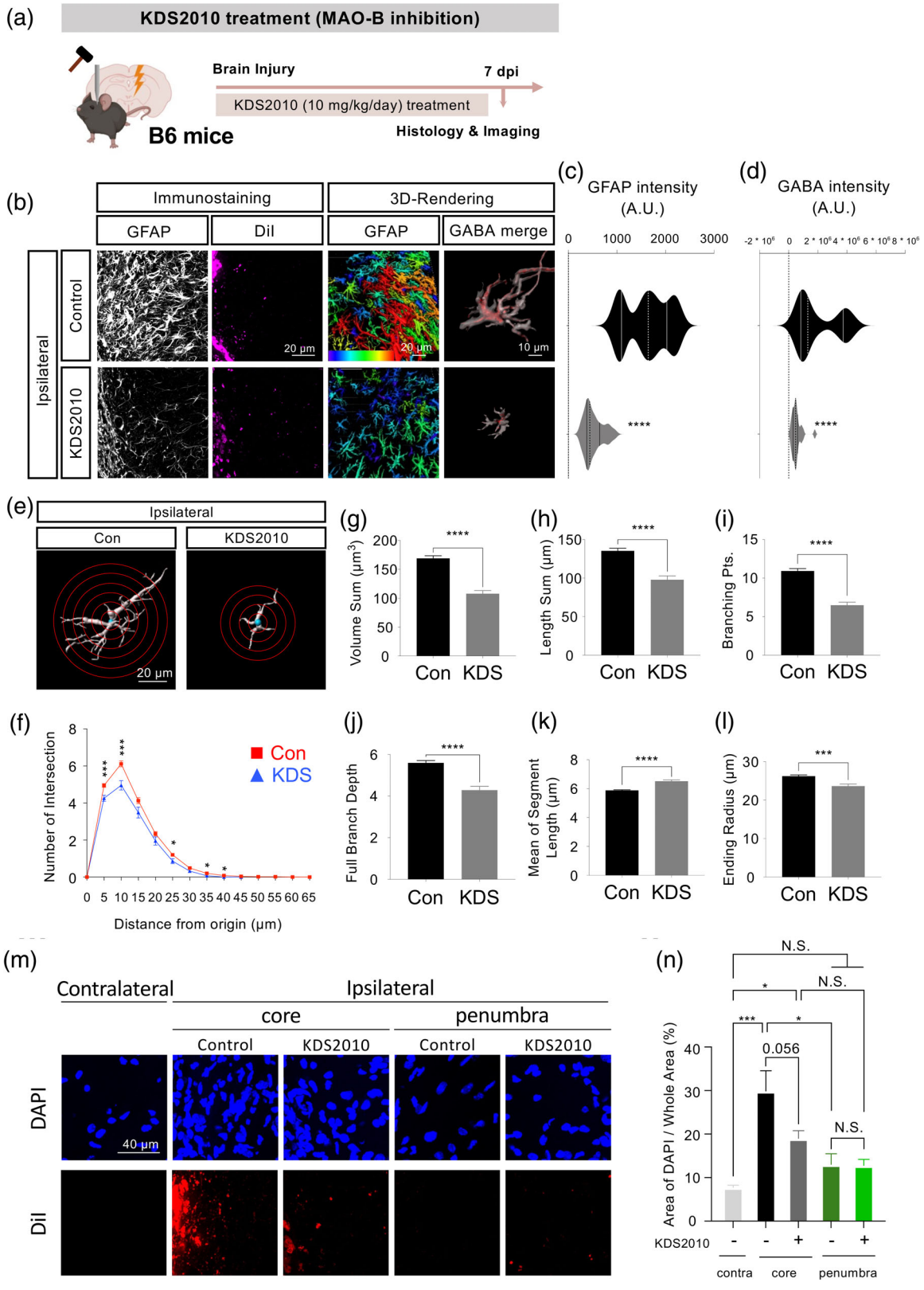

FIGURE 4 Legend on next page.

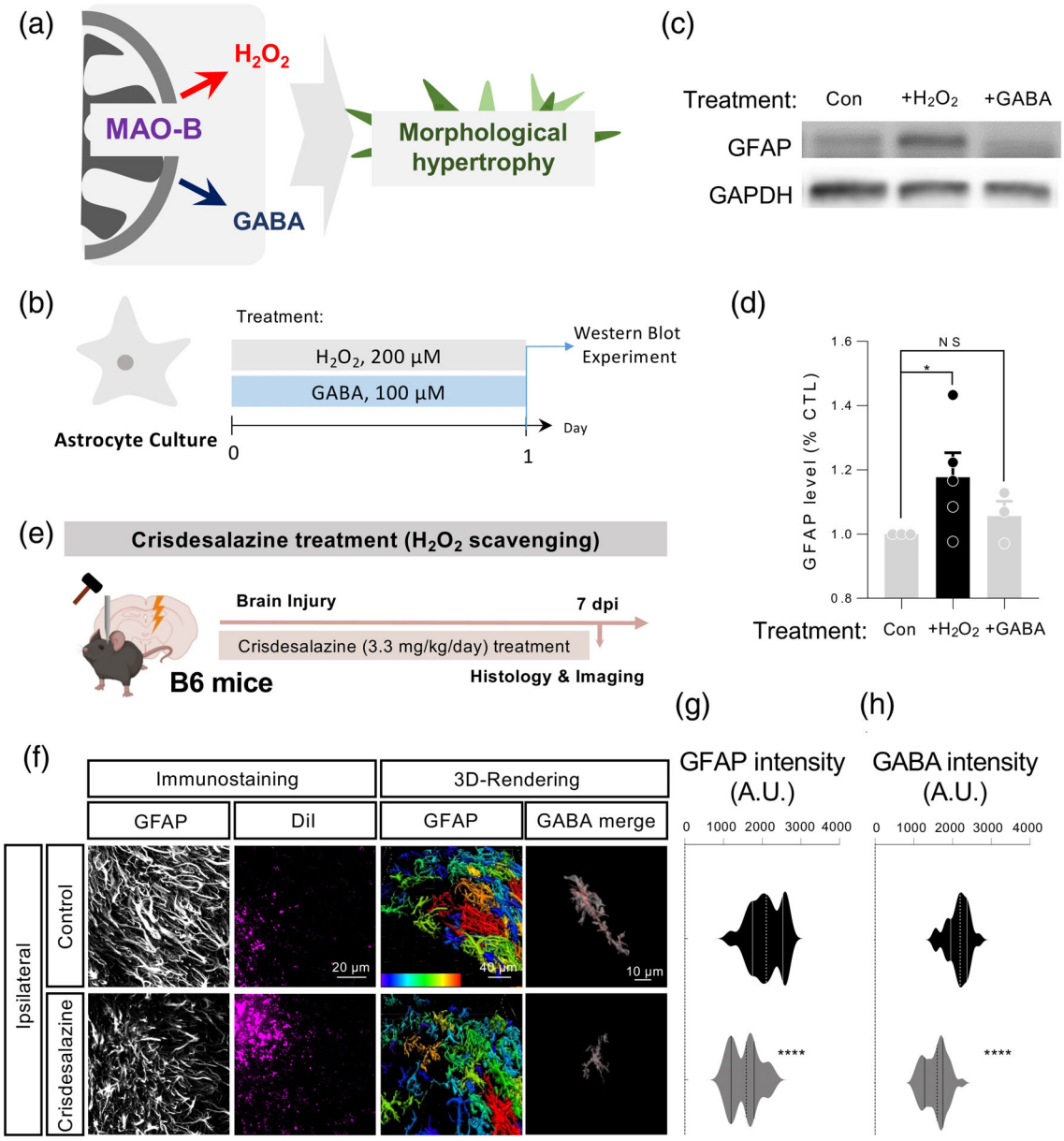

FIGURE 5 H_2O_2, not gamma-aminobutyric acid (GABA), is involved in the reactivity of astrocytes. (a) Proposed mechanism of morphological hypertrophy mediated by monoamine oxidase B (MAO-B) activity in reactive astrocytes of STAB. (b) Experimental timeline for H_2O_2 or GABA treatment in cultured astrocytes. (c,d) Western blot and quantification for glial fibrillary acidic protein (GFAP) expression in H_2O_2- or GABA-treated cultured astrocytes. (e) Experimental timeline for STAB and crisdesalazine (AAD-2004) administration in B6 mice. (f) Representative confocal images for GFAP and DiI (left) and the 3D-rendered images for GFAP pseudo-colored by volume (value range: 0–8000) and GABA (right) in crisdesalazine-treated STAB model. (g,h) Violin plot showing the average intensity of GFAP (g) and GABA (h) immunoreacitivity in CA1 stratum radiatum of crisdesalazine-treated STAB model. Data are presented as the mean ± SEM (*p < .05, ****p < .0001)

FIGURE 4 The pharmacological attenuation of scar-forming severe reactive astrocytes of STAB by KDS2010 administration. (a) Experimental timeline for STAB and KDS2010 administration in B6 mice. (b) Representative confocal images for GFAP and DiI (left) and the 3D-rendered images for GFAP pseudocolored by volume (value range: 0–8000) and GABA (right) in STAB model with KDS2010 treatment. (c,d) Violin plot showing the average intensity of GFAP (c) and GABA (d) immunoreacitivity in CA1 stratum radiatum of STAB with KDS2010 treatment. (e) Representative images of sholl analysis in astrocytes of STAB model with KDS2010 treatment. (f) Measurement of the number of intersection according to the distance from the nucleus through sholl analysis. (g–l) Measurement of the volume sum (g), the length sum (h), the branching points (i), the full branch depth (j), the mean of segment length (k) and the ending radius (l). (m) Representative images of DAPI and DiI signals in STAB model with KDS 2010 treatment. (n) Measurement of percentage of area of DAPI signals. Data are presented as the mean ± SEM (*p < .05, **p < .01, ***p < .001, ****p < .0001)

As a result, the increased astrocytic GABA and GFAP signals by injury on the ipsilateral side were significantly attenuated by KDS2010 treatment (Figure 4b–d). Further analysis using filament tracing showed that the astrocytes in the KDS2010-treated mice displayed a significant reduction in complexity compared to that in WT mice (Figure 4e–l). The number of intersections and the sum of process volume/length, as well as the number of branching points and the full branch depth, were significantly decreased in the KDS2010 condition compared to the control condition. Furthermore, the mean of segment length was significantly increased in the KDS2010-treated condition (Figure 4e–l). These results indicate that the effect of KDS2010 on the GFAP and GABA expression and complexity of astrocytes was as dramatic as in the case of genetic knockout of MAO-B. To assess the proliferative potential of the injured area, the DAPI signal was analyzed in the core and penumbral regions (Figure 4m). We found that the percentage of area of DAPI signal was significantly higher in the core region, but not in the penumbra region (Figure 4n), whereas the higher DAPI signal was significantly attenuated by KDS2010 treatment (Figure 4m,n), suggesting that the core region contains highly proliferative reactive astrocytes, which is significantly reversed by MAO-B inhibition. Taken together, these results raise KDS2010 as a promising therapeutic candidate for brain injury by blocking the scar-forming severe reactive astrocytes.

3.4 | H_2O_2-mediated mechanism of scar-forming severe reactive astrocytes in STAB

MAO-B is a family of oxidases and the action of MAO-B in astrocytes produces hydrogen peroxide, H_2O_2, and GABA in the process of degradation of acetyl-putrescine. To examine the key element which plays a major role in modulating the morphological reactivity of astrocytes among two byproducts of MAO-B activation, we treated GABA or H_2O_2 in cultured astrocytes and measured the level of astrocytic

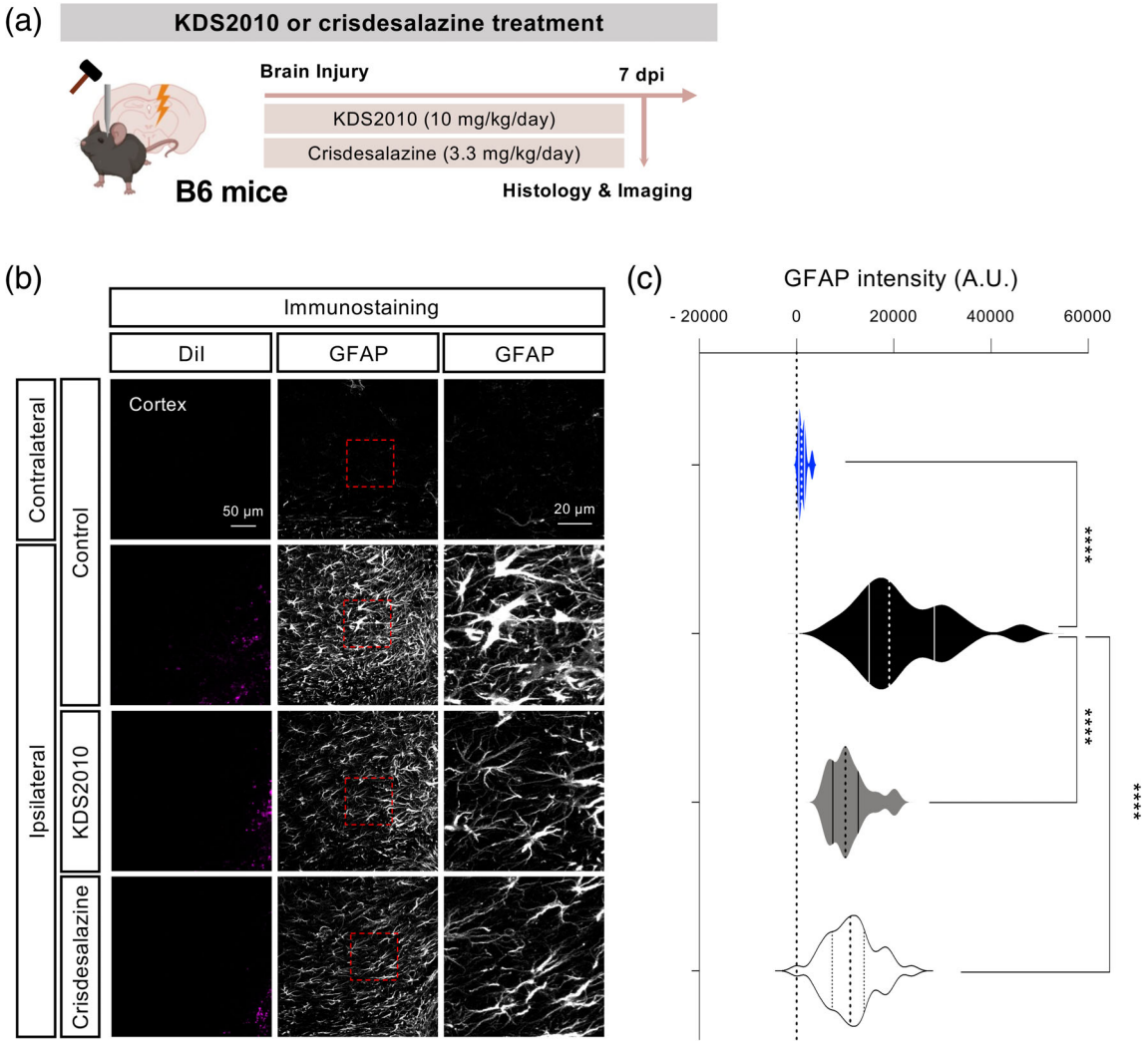

FIGURE 6 Cortical astrocytes share common monoamine oxidase B/gamma-aminobutyric acid/H_2O_2 pathway in the STAB model. (a) Experimental timeline for STAB and KDS2010 and crisdesalazine administration in B6 mice. (b) Representative confocal images for DiI and GFAP in KDS2010 and crisdesalazine-treated STAB model. (c) Violin plot showing the average intensity of GFAP immunoreacitivity in cortex of KDS2010 and crisdesalazine-treated STAB model. Data are presented as the mean ± SEM (****$p < .0001$)

cytoskeletal protein, GFAP (Figure 5a,b). As a result, the level of GFAP protein was significantly increased in H_2O_2-treated astrocytes, but not in GABA-treated astrocytes (Figure 5c,d). These results indicate that H_2O_2, rather than GABA, is a possible molecule involved in the morphological hypertrophy of astrocytes in the STAB model. Importantly, a recent study also showed that H_2O_2 produced in reactive astrocytes of AD models such as GiD and APP/PS1 plays a crucial role in memory impairment and in astrocytic reactivity (Chun et al., 2020). To test the effect of H_2O_2 on the morphological reactivity of astrocytes in the STAB model, we applied crisdesalazine (3.3 mg/kg/day), a potent H_2O_2 scavenger (Chun et al., 2020), for 7 days in the STAB model and assessed the morphological alterations in the scar region near the injury site. As a result, the level of GFAP was significantly reduced in the crisdesalazine-treated group, compared to that in the control group (Figure 5e–g). These results indicate that H_2O_2 is a key molecule for the morphological hypertrophy of reactive astrocytes in the STAB model. In addition, the GABA expression in each astrocyte was significantly decreased in the cridsdesalazine-treated condition, suggesting that H_2O_2 is also important for GABA production or clearance or both.

3.5 | Common monoamine oxidase B/gamma-aminobutyric acid/H_2O_2 pathway in cortical astrocytes of STAB

Astrocytes are highly heterogenous, even in the same brain region (Matias et al., 2019). To investigate whether MAO-B inhibitor and H_2O_2 scavenger also have an effect on the different brain region, we measured the GFAP signal in the cortex right above the CA1 hippocampus (Figure 6a). As a result, GFAP signal was very low in the contralateral side, but the STAB model induced significantly higher expression of GFAP along with hypertrophy and scar formation. The hypertrophy and scar formation of astrocytes were significantly attenuated by KDS 2010 and crisdesalazine treatment, consistent with the results from the hippocampus (Figure 6b,c). These results demonstrate

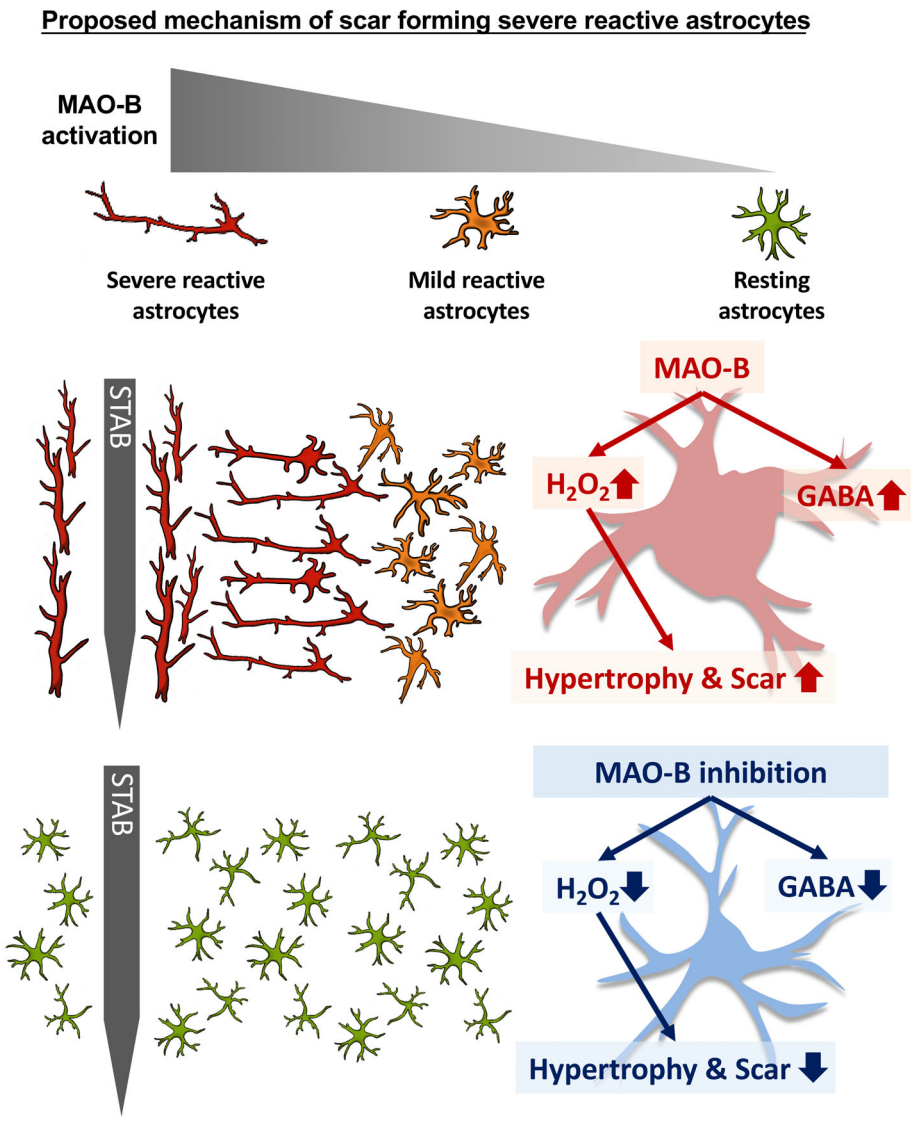

FIGURE 7 Schematic diagram of proposed mechanism for inducing reactive astrocytes in brain injury model. The morphological hypertrophy and scar formation of reactive astrocytes is attributed to monoamine oxidase B (MAO-B) action and its byproduct, H_2O_2, in STAB model, implicating that inhibiting MAO-B activity has dual beneficial effects of reducing astrogliosis and transforming reactive astrocytes into resting astrocytes under pathological conditions

that hypertrophy and scar formation of hippocampal and cortical astrocytes are mediated by common MAO-B/GABA/H_2O_2 pathway.

4 | DISCUSSION

In this study, we investigated how the morphological hypertrophy of reactive astrocytes is induced in a stab wound injury model. Our study was based on previous observations showing increased astrocytic GABA and tonic inhibition in a brain injury model and the MAO-B-mediated reactive astrocytes in various brain diseases such as Parkinson's disease, Alzheimer's disease and stroke (Heo et al., 2020; Jo et al., 2014; Nam, Cho, et al., 2020). We examined whether the common molecular pathway of reactive astrocytes is shared by scar-forming reactive astrocytes in a brain injury model. Moreover, we focused on the detailed molecular mechanism of whether and how MAO-B can be involved in the structural hypertrophy of scar-forming reactive astrocytes. In this study, we provide a plausible explanation for how the MAO-B induces astrocytic scar and demonstrate that, among the two by-products of MAO-B activation, H_2O_2, but not GABA, is responsible for the morphological hypertrophy of reactive astrocytes in the penetrating brain injury model. We hypothesize that H_2O_2 may cause epigenetic alterations during the formation of proliferating severe reactive astrocytes. H_2O_2-mediated gene expression changes and the related molecular pathways might increase the expression of hypertrophy-related structural proteins such GFAP. In addition, we have previously shown that microglial activation is mediated by MAO-B dependent astrocytic H_2O_2 in Alzheimer's disease mouse model (Chun et al., 2020). Based on our previous study, the level of microglia activity should be attenuated by MAO-B inhibition and H_2O_2 scavenger. The investigation of these exciting topics will be the next step.

Previous reports have shown that the penetrating brain injury acutely increases infiltration of blood, immune cells and cytokines and causes severe inflammation by direct tissue damage (DiSabato et al., 2016). The series of events after injury is postulated to cause glial activation and induce a glial scar barrier. However, the origin of scar-forming reactive astrocytes is being debated as to whether the increased number of GFAP-positive cells is derived from resting astrocytes or from other cell types such as stem cells. In this study, we demonstrated that the common MAO-B-mediated pathway induces proliferating scar-forming reactive astrocytes near the injured region, and severe reactive astrocytes can be attenuated by MAO-B inhibition. These results implicate the possibility that resident astrocytes, not other cell types, are transformed into a proliferating form in a graded manner. Additionally, our study implies that environments or critical factors of the injured region may activate the putrescine-degradative MAO-B pathway in astrocytes. Determining the activator of the MAO-B pathway is an interesting topic that should be pursued in future studies.

In the field of glial biology, there is a pressing need to establish criteria for distinguishing the subtypes of reactive astrocytes. We have recently proposed that at least two fundamentally different reactive astrocytes can be readily distinguished by the degree of MAO-B activation: (1) Irreversible severe reactive astrocytes, which are extremely hypertrophied, producing excessive GABA and H_2O_2 and highly proliferating, and (2) reversible mild reactive astrocytes, which are moderately hypertrophied, producing GABA and H_2O_2, but not excessively, and non-proliferating. In this study, we also observed the presence of the severe reactive astrocytes in the core region of injury, which are highly hypertrophied with scar formation, producing GABA excessively and proliferating. These features all require MAO-B activation. In contrast, we observed the presence of the mild reactive astrocytes in the penumbra region, which are moderately hypertrophied and producing GABA. These features also require MAO-B activation at moderate level. Our results suggest that the transformation from resting astrocytes to mild reactive astrocytes to scar-forming severe reactive astrocyte is dependent on the degree of MAO-B activation in a graded fashion (Figure 7). Based on these findings, we have established a new practical criterion for distinguishing the severity of reactive astrocytes by measuring the degree of MAO-B activation.

In traumatic CNS injury, it has been controversial whether scar-forming reactive astrocytes are detrimental or beneficial. First, regarding scar formation as a detrimental symptom, the widespread view on the scar-forming reactive astrocytes is that glial scar primarily acts as a mechanical barrier to prevent axon regeneration of injured neurons (Yang et al., 2020). It is known that the proliferating scar-forming reactive astrocytes form fences and isolate the damaged region from the relatively distant viable brain tissue. Contrary to this negative view, studies have reported that the loss of scar-forming reactive astrocytes using cell-ablating systems such as GFAP-TK mice or the STAT3 KO model leads to attenuated axon regeneration, the increased spread of inflammation and decreased functional recovery, suggesting the beneficial function of proliferating reactive astrocytes (Anderson et al., 2016). Moreover, another group also suggested that the rod-like scar-forming reactive astrocytes probably act as a bridge to guide the crushed neuron and to support axon regeneration called, 'astrocyte-bridge' (Sun et al., 2011; Zukor et al., 2013). The reason for this continuing controversy is probably due to the lack of appropriate tools to control reactivity of astrocytes. In this study, we have delineated how the genetic and pharmacological MAO-B inhibition can transform detrimental reactive astrocytes into resting astrocytes in the injured brain. We have demonstrated that genetic deletion of MAO-B, MAO-B inhibitor or H_2O_2 scavenger reduces hypertrophy and scar formation of reactive astrocytes. These genetic and pharmacological tools that we have established in this study will prove useful in resolving the controversial views on opposing roles of scar-forming reactive astrocytes in the CNS injury.

ACKNOWLEDGMENTS

This work was supported by the Institute for Basic Science (IBS), Center for Cognition and Sociality (IBS-R001-D2). We are grateful to Dr. Byoung Joo Gwag from GNT Pharma for providing crisdesalazine (AAD-2004) and Dr. Ki Duk Park for providing KDS2010.

CONFLICT OF INTEREST

The authors declare no conflict of interest.

AUTHOR CONTRIBUTIONS

Heejung Chun, Jiwoon Lim and C. Justin Lee designed the study and wrote the manuscript. Heejung Chun and Jiwoon Lim performed and analyzed the IHC. Heejung Chun performed and analyzed the western blot. All authors contributed to the analysis and discussion of the results and reviewed the manuscript.

DATA AVAILABILITY STATEMENT

The datasets generated for the main figures are available from the corresponding author upon reasonable request.

ORCID

C. Justin Lee https://orcid.org/0000-0002-3555-0980

REFERENCES

Anderson, M. A., Burda, J. E., Ren, Y., Ao, Y., O'Shea, T. M., Kawaguchi, R., & Sofroniew, M. V. (2016). Astrocyte scar formation aids central nervous system axon regeneration. *Nature*, *532*(7598), 195–200. https://doi.org/10.1038/nature17623

Bourguignon, L. Y., Gilad, E., Peyrollier, K., Brightman, A., & Swanson, R. A. (2007). Hyaluronan-CD44 interaction stimulates Rac1 signaling and PKN gamma kinase activation leading to cytoskeleton function and cell migration in astrocytes. *Journal of Neurochemistry*, *101*(4), 1002–1017. https://doi.org/10.1111/j.1471-4159.2007.04485.x

Chun, H., An, H., Lim, J., Woo, J., Lee, J., Ryu, H., & Lee, C. J. (2018). Astrocytic proBDNF and tonic GABA distinguish active versus reactive astrocytes in hippocampus. *Experimental Neurobiology*, *27*(3), 155–170. https://doi.org/10.5607/en.2018.27.3.155

Chun, H., Im, H., Kang, Y. J., Kim, Y., Shin, J. H., Won, W., Lim, J., Ju, Y., Park, Y. M., Kim, S., Lee, S. E., Lee, J., Woo, J., Hwang, Y., Cho, H., Jo, S., Park, J.-H., Kim, D., Kim, D. Y., … Lee, C. J. (2020). Severe reactive astrocytes precipitate pathological hallmarks of Alzheimer's disease via $H_2O_2^-$ production. *Nature Neuroscience*, *23*(12), 1555–1566. https://doi.org/10.1038/s41593-020-00735-y

DiSabato, D. J., Quan, N., & Godbout, J. P. (2016). Neuroinflammation: The devil is in the details. *Journal of Neurochemistry*, *139*(Suppl 2), 136–153. https://doi.org/10.1111/jnc.13607

Ekblom, J., Jossan, S. S., Bergstrom, M., Oreland, L., Walum, E., & Aquilonius, S. M. (1993). Monoamine oxidase-B in astrocytes. *Glia*, *8*(2), 122–132. https://doi.org/10.1002/glia.440080208

Escartin, C., Galea, E., Lakatos, A., O'Callaghan, J. P., Petzold, G. C., Serrano-Pozo, A., Steinhäuser, C., Volterra, A., Carmignoto, G., Agarwal, A., Allen, N. J., Araque, A., Barbeito, L., Barzilai, A., Bergles, D. E., Bonvento, G., Butt, A. M., Chen, W. T., Cohen-Salmon, M., … Verkhratsky, A. (2021). Reactive astrocyte nomenclature, definitions, and future directions. *Nature Neuroscience*, *24*(3), 312–325. https://doi.org/10.1038/s41593-020-00783-4

Escartin, C., Guillemaud, O., & Carrillo-de Sauvage, M. A. (2019). Questions and (some) answers on reactive astrocytes. *Glia*, *67*(12), 2221–2247. https://doi.org/10.1002/glia.23687

Heo, J. Y., Nam, M. H., Yoon, H. H., Kim, J., Hwang, Y. J., Won, W., Woo, D. H., Lee, J. A., Park, H. J., Jo, S., Lee, M. J., Kim, S., Shim, J. E., Jang, D. P., Kim, K. I., Huh, S. H., Jeong, J. Y., Kowall, N. W., Lee, J., … Lee, C. J. (2020). Aberrant tonic inhibition of dopaminergic neuronal activity causes motor symptoms in animal models of Parkinson's disease. *Current Biology*, *30*(2), 276–291. https://doi.org/10.1016/j.cub.2019.11.079

Jo, S., Yarishkin, O., Hwang, Y. J., Chun, Y. E., Park, M., Woo, D. H., Bae, J. Y., Kim, T., Lee, J., Chun, H., Park, H. J., Lee, D. Y., Hong, J., Kim, H. Y., Oh, S. J., Park, S. J., Lee, H., Yoon, B. E., Kim, Y., … Lee, C. J. (2014). GABA from reactive astrocytes impairs memory in mouse models of Alzheimer's disease. *Nature Medicine*, *20*(8), 886–896. https://doi.org/10.1038/nm.3639

Li, K., Li, J., Zheng, J., & Qin, S. (2019). Reactive astrocytes in neurodegenerative diseases. *Aging and Disease*, *10*(3), 664–675. https://doi.org/10.14336/AD.2018.0720

Liddelow, S. A., Guttenplan, K. A., Clarke, L. E., Bennett, F. C., Bohlen, C. J., Schirmer, L., Bennett, M. L., Münch, A. E., Chung, W.-S., Peterson, T. C., Wilton, D. K., Frouin, A., Napier, B. A., Panicker, N., Kumar, M., Buckwalter, M. S., Rowitch, D. H., Dawson, V. L., Dawson, T. M., … Barres, B. A. (2017). Neurotoxic reactive astrocytes are induced by activated microglia. *Nature*, *541*(7638), 481–487. https://doi.org/10.1038/nature21029

Maggiorani, D., Manzella, N., Edmondson, D. E., Mattevi, A., Parini, A., Binda, C., & Mialet-Perez, J. (2017). Monoamine oxidases, oxidative stress, and altered mitochondrial dynamics in cardiac ageing. *Oxidative Medicine and Cellular Longevity*, *2017*, 3017947. https://doi.org/10.1155/2017/3017947

Mallajosyula, J. K., Kaur, D., Chinta, S. J., Rajagopalan, S., Rane, A., Nicholls, D. G., Di Monte, D. A., Macarthur, H., & Andersen, J. K. (2008). MAO-B elevation in mouse brain astrocytes results in Parkinson's pathology. *PLoS One*, *3*(2), e1616. https://doi.org/10.1371/journal.pone.0001616

Matias, I., Morgado, J., & Gomes, F. C. A. (2019). Astrocyte heterogeneity: Impact to brain aging and disease. *Frontiers in Aging Neuroscience*, *11*, 1–18. https://doi.org/10.3389/fnagi.2019.00059

Matyash, M., Matyash, V., Nolte, C., Sorrentino, V., & Kettenmann, H. (2002). Requirement of functional ryanodine receptor type 3 for astrocyte migration. *The FASEB Journal*, *16*(1), 84–86. https://doi.org/10.1096/fj.01-0380fje

McGraw, J., Hiebert, G. W., & Steeves, J. D. (2001). Modulating astrogliosis after neurotrauma. *Journal of Neuroscience Research*, *63*(2), 109–115. https://doi.org/10.1002/1097-4547(20010115)63:2<109::AID-JNR1002>3.0.CO;2-J

Menet, V., Prieto, M., Privat, A., & Gimenez y Ribotta, M. (2003). Axonal plasticity and functional recovery after spinal cord injury in mice deficient in both glial fibrillary acidic protein and vimentin genes. *Proceedings of the National Academy of Sciences of the United States of America*, *100*(15), 8999–9004. https://doi.org/10.1073/pnas.1533187100

Nam, M. H., Cho, J., Kwon, D. H., Park, J. Y., Woo, J., Lee, J. M., Lee, S., Ko, H. Y., Won, W., Kim, R. G., Song, H., Oh, S. J., Choi, J. W., Park, K. D., Park, E. K., Jung, H., Kim, H. S., Lee, M. C., Yun, M., … Kim, H. I. (2020). Excessive astrocytic GABA causes cortical Hypometabolism and impedes functional recovery after subcortical stroke. *Cell Reports*, *32*(3), 107975. https://doi.org/10.1016/j.celrep.2020.107975

Nam, M.-H., Park, J.-H., Song, H. J., Choi, J. W., Kim, S., Jang, B. K., Hoon, H. H., Heo, J. Y., Cho, D.-W., Yang, Y.-S., Han, S.-C., Kim, S., Oh, S.-J., Jeon, S. R., & Park, K. D. (2021). KDS2010, a newly developed reversible MAO-B inhibitor, as an effective therapeutic candidate for Parkinson's disease. *Neurotherapeutics*, 1–19. https://doi.org/10.1007/s13311-021-01097-4

Park, J. H., Ju, Y. H., Choi, J. W., Song, H. J., Jang, B. K., Woo, J., Chun, H., Kim, H. J., Shin, S. J., Yarishkin, O., Jo, S., Park, M., Yeon, S. K., Kim, S., Kim, J., Nam, M. H., Londhe, A. M., Kim, J., Cho, S. J., … Park, K. D. (2019). Newly developed reversible MAO-B inhibitor circumvents the shortcomings of irreversible inhibitors in Alzheimer's disease. *Science Advances*, *5*(3), eaav0316. https://doi.org/10.1126/sciadv.aav0316

Sofroniew, M. V. (2009). Molecular dissection of reactive astrogliosis and glial scar formation. *Trends in Neurosciences*, *32*(12), 638–647. https://doi.org/10.1016/j.tins.2009.08.002

Sun, F., Park, K. K., Belin, S., Wang, D., Lu, T., Chen, G., Zhang, K., Yeung, C., Feng, G., Yankner, B. A., & He, Z. (2011). Sustained axon

regeneration induced by co-deletion of PTEN and SOCS3. *Nature*, *480*(7377), 372–375. https://doi.org/10.1038/nature10594

Tong, J., Rathitharan, G., Meyer, J. H., Furukawa, Y., Ang, L. C., Boileau, I., Guttman, M., Hornykiewicz, O., & Kish, S. J. (2017). Brain monoamine oxidase B and a in human parkinsonian dopamine deficiency disorders. *Brain*, *140*(9), 2460–2474. https://doi.org/10.1093/brain/awx172

Verkhratsky, A., Ho, M. S., Vardjan, N., Zorec, R., & Parpura, V. (2019). General pathophysiology of astroglia. *Advances in Experimental Medicine and Biology*, *1175*, 149–179. https://doi.org/10.1007/978-981-13-9913-8_7

Yang, T., Dai, Y., Chen, G., & Cui, S. (2020). Corrigendum: Dissecting the dual role of the glial scar and scar-forming astrocytes in spinal cord injury. *Frontiers in Cellular Neuroscience*, *14*, 270. https://doi.org/10.3389/fncel.2020.00270

Yoon, B. E., Woo, J., Chun, Y. E., Chun, H., Jo, S., Bae, J. Y., An, H., Min, J. O., Oh, S. J., Han, K. S., Kim, H. Y., Kim, T., Kim, Y. S., Bae, Y. C., & Lee, C. J. (2014). Glial GABA, synthesized by monoamine oxidase B, mediates tonic inhibition. *The Journal of Physiology*, *592*(22), 4951–4968. https://doi.org/10.1113/jphysiol.2014.278754

Yun, S. P., Kam, T. I., Panicker, N., Kim, S., Oh, Y., Park, J. S., Kwon, S. H., Park, Y. J., Karuppagounder, S. S., Park, H., Kim, S., Oh, N., Kim, N. A., Lee, S., Brahmachari, S., Mao, X., Lee, J. H., Kumar, M., An, D., … Ko, H. S. (2018). Block of A1 astrocyte conversion by microglia is neuroprotective in models of Parkinson's disease. *Nature Medicine*, *24*(7), 931–938. https://doi.org/10.1038/s41591-018-0051-5

Zhang, Y., & Barres, B. A. (2010). Astrocyte heterogeneity: An underappreciated topic in neurobiology. *Current Opinion in Neurobiology*, *20*(5), 588–594. https://doi.org/10.1016/j.conb.2010.06.005

Zukor, K., Belin, S., Wang, C., Keelan, N., Wang, X., & He, Z. (2013). Short hairpin RNA against PTEN enhances regenerative growth of corticospinal tract axons after spinal cord injury. *The Journal of Neuroscience*, *33*(39), 15350–15361. https://doi.org/10.1523/JNEUROSCI.2510-13.2013

SUPPORTING INFORMATION

Additional supporting information may be found in the online version of the article at the publisher's website.

How to cite this article: Chun, H., Lim, J., Park, K. D., & Lee, C. J. (2021). Inhibition of monoamine oxidase B prevents reactive astrogliosis and scar formation in stab wound injury model. *Glia*, 1–14. https://doi.org/10.1002/glia.24110